

STOCHASTIC HAZARD DETECTION FOR LANDING UNDER TOPOGRAPHIC UNCERTAINTY

Kento Tomita*, Koki Ho†

Autonomous hazard detection and avoidance is a key technology for future landing missions in unknown surface conditions. Current state-of-the-art stochastic algorithms assume simple Gaussian measurement noise on dense, high-fidelity digital elevation maps, limiting the algorithm’s applicability. This paper introduces a new stochastic hazard detection algorithm capable of more general topographic uncertainty by leveraging the Gaussian random field regression. The proposed approach enables the safety assessment with imperfect and sparse sensor measurements, which allows hazard detection operations under more diverse conditions. We demonstrate the performance of the proposed approach on the existing Mars digital terrain models.

INTRODUCTION

Autonomous hazard detection and avoidance (HD&A) is a key technology for future landing missions in unknown surface conditions. Current state-of-the-art autonomous HD&A algorithms require dense, high-fidelity digital elevation maps (DEMs), and often assume a simple Gaussian error on the range measurements.¹ We propose a new hazard detection (HD) algorithm capable of more general topographic uncertainty by leveraging the Gaussian random field (GRF) regression to reduce reliance on expensive, high-fidelity, dense terrain maps.

Previous works^{1,2} on the uncertainty-aware HD algorithms mainly studied the effect of the range error of LiDAR sensors. Ivanov et al.¹ developed a probabilistic HD algorithm assuming the identically and independently distributed Gaussian error on the LiDAR’s range measurement, given the lander geometry and navigation errors. Tomita et al.² applied Bayesian deep learning techniques to solve the same problem with increased performance. However, the previous works^{1,2} assume noisy but dense DEMs, and do not incorporate the topographic uncertainty caused by the sparsity of the LiDAR measurements. LiDAR sensors measure the distance to the terrain surface, and output point cloud data (PCD), which is the collection of the estimated coordinates of the measured points on the surface. The maximum ground sample distance (GSD) of PCD increases at higher altitudes or by non-orthogonal observations, which causes the blank spots on the obtained DEMs.³ Figure 1 shows the simulated DEMs have missing data due to the large slant range or angle. To handle PCD with larger GSDs than the required DEM resolution, we leverage the Gaussian random field regression to estimate the dense DEM with appropriate uncertainty, and derive the probability of safety for each surface point.

The contributions of this paper are as follows: first, we develop a new stochastic hazard detection algorithm that leverages the Gaussian random field (GRF) to accurately predict safety probability

*PhD Student, School of Aerospace Engineering, Georgia Institute of Technology, Atlanta, GA 30313, USA.

†Associate Professor, School of Aerospace Engineering, Georgia Institute of Technology, Atlanta, GA 30313, USA.

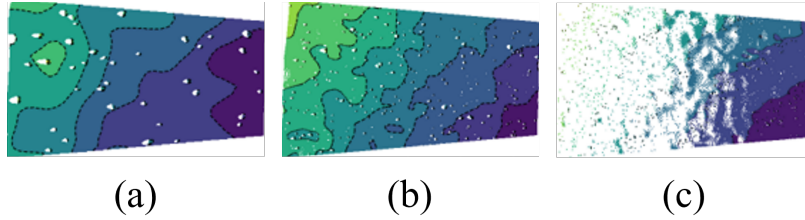


Figure 1. Simulated DEMs over the slant ranges of (a) 100m, (d) 250m, and (c) 500m. The LiDAR detector size is 1024x1024 and slant angle is set 30 deg. There are holes due to the rock occultations with the large slant angle in (a) and (b) and the extended ground-sample-distances due to the large slant range and angle in (c).

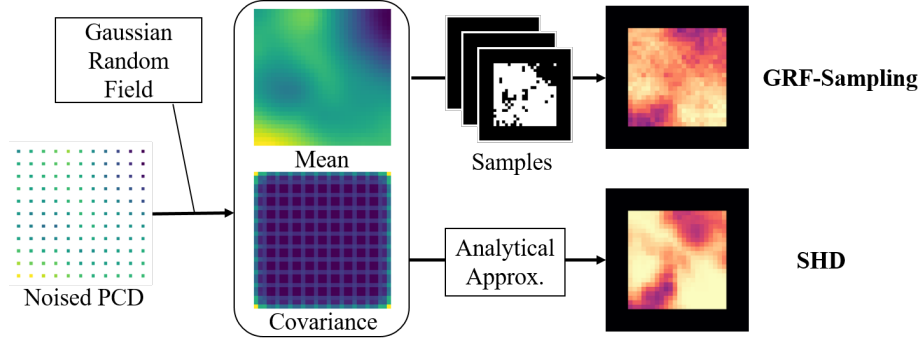


Figure 2. Pipeline of the proposed approach.

from noisy and sparse LiDAR measurements; second, we derive the analytic form of the approximated probability of safety under the GRF representation of the terrain; and third, we demonstrate and analyze the performance of the proposed approach on real Mars digital terrain models.

PROPOSED APPROACH

Terrain Approximation by Gaussian Random Fields

We approximate the topography of the target terrain by a Gaussian random field (GRF), which is a joint Gaussian distribution about the surface elevations, also referred to as a two-dimensional Gaussian process.⁴ Specifically, let $\gamma_i = [x_i, y_i]^T \in \mathcal{S}$ be the horizontal position of an arbitrary surface point where $\mathcal{S} \subseteq \mathbb{R}^2$ is the horizontal projection of all the surface points of our interest. Then, by the GRF approximation, we assume that the elevations $\{z_i = f(\gamma_i) | \gamma_i \in \mathcal{S}\}$ are jointly Gaussian such that

$$\mathbb{E}[f(\gamma_i)] = \mu_i, \quad \mathbb{E}[(f(\gamma_i) - \mu_i)(f(\gamma_j) - \mu_j)] = k(\gamma_i, \gamma_j), \quad \forall i, j = 1, 2, \dots, |\mathcal{S}| \quad (1)$$

for the appropriately chosen mean μ_i and the kernel function, $k(\gamma_i, \gamma_j)$. We use the absolute exponential kernel function to approximate natural terrains by a Brownian motion^{5,6}

$$k(\gamma_i, \gamma_j) = u \exp\left(-\frac{\|\gamma_i - \gamma_j\|}{\ell}\right) \quad (2)$$

where $u > 0$ and $\ell > 0$ are the hyperparameters of the GRF.

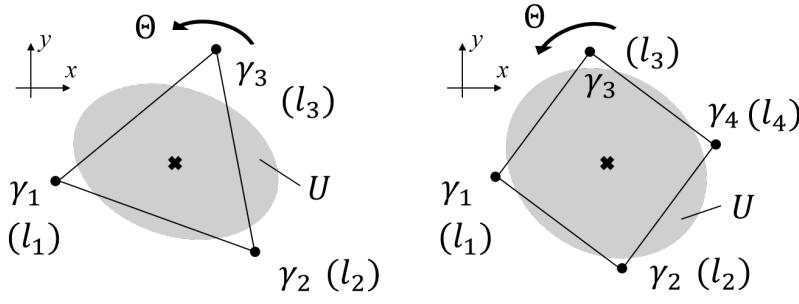


Figure 3. Schematics of the triangular and square lander geometries. The bold cross mark at the center is the target whose landing safety is evaluated. We evaluate all the possible landing pad placements over different orientation angles θ . The gray area denoted by U is the lander footprint where roughness safety is evaluated.

Given the terrain measurements, whether noisy or sparse, we can condition the GRF on the measurements. Suppose we have n noisy observed elevations of the terrain, $\mathbf{z} = [z_1, z_2, \dots, z_n]^T$, for the horizontal locations of $\Gamma = [\gamma_1, \gamma_2, \dots, \gamma_n]^T$. We would like to obtain n_* elevations of $\mathbf{z}_* = [z_{1*}, z_{2*}, \dots, z_{n*}]^T$ for $\Gamma_* = [\gamma_{1*}, \gamma_{2*}, \dots, \gamma_{n*}]^T$. Let σ^2 be the variance of the Gaussian observation noise, then we have the conditional distribution⁴

$$\begin{aligned} \mathbf{z}_* | \Gamma, \mathbf{z}, \Gamma_* &\sim \mathcal{N}(\bar{\mathbf{z}}_*, \text{cov}(\mathbf{z}_*)), \quad \text{where} \\ \bar{\mathbf{z}}_* &:= \mathbb{E}[\mathbf{z}_* | \Gamma, \mathbf{z}, \Gamma_*] = K(\Gamma_*, \Gamma) [K(\Gamma, \Gamma) + \sigma^2 I]^{-1} \mathbf{z} \\ \text{cov}(\mathbf{z}_*) &= K(\Gamma_*, \Gamma_*) - K(\Gamma_*, \Gamma) [K(\Gamma, \Gamma) + \sigma^2 I]^{-1} K(\Gamma, \Gamma_*). \end{aligned} \quad (3)$$

Here $K(\gamma_*, \gamma) \in \mathbb{R}^{n_* \times n}$ is the covariance matrix whose i, j entry corresponds to $k(\gamma_i, \gamma_{j*})$, and similar for $K(\gamma, \gamma)$, $K(\gamma, \gamma_*)$, and $K(\gamma_*, \gamma_*)$. To optimize the hyperparameters of k , we maximize the log marginal likelihood⁴

$$\log p(\mathbf{z} | \Gamma) = -\frac{1}{2} \mathbf{z}^T (K + \sigma^2 I)^{-1} \mathbf{z} - \frac{1}{2} \log |K + \sigma^2 I| - \frac{n}{2} \log 2\pi \quad (4)$$

where $K = K(\Gamma, \Gamma)$. For more details about the Gaussian random field regression, please refer to Reference 4.

Probability of Landing Safety

Given the GRF representation of the dense elevation map, we compute the slope and roughness at touchdown, which defines the landing safety. Suppose we have a target site whose landing safety is to be evaluated, then the slope and roughness depend on the lander's orientation angle, $\theta_o \in \Theta$, as shown in Figure 3. We classify the target as safe if the slope and roughness are under the given thresholds for all the orientation angles. Therefore, the probability of safety for the target is the joint probability of $\{\text{Safe} | \theta_o\}$ over $\theta_o \in \Theta$, which is the safety given the orientation angle θ . Under the GRF representation of the terrain, safety for each θ_o is not independent, and the precise computation of the joint probability is not straightforward. Instead, we approximate the joint probability by the worst-case safety probability with the raising factor of $k_1 > 0$, as shown in Eq. (5).

$$\begin{aligned} \mathbb{P}(\text{Safe}) &= \mathbb{P}\{\text{Safe} | \theta_1, \text{Safe} | \theta_2, \dots, \text{Safe} | \theta_{|\Theta|}\} \\ &\sim \left[\min_{\theta_o \in \Theta} \mathbb{P}\{\text{Safe} | \theta_o\} \right]^{k_1} \end{aligned} \quad (5)$$

To compute $\mathbb{P}\{\text{Safe}|\theta_o\}$, let $l_1, l_2, l_3 \in \mathbb{R}^3$ be the position of the three landing pads contacting with the terrain with the orientation angle θ_o .

$$l_1 = [x_1, y_1, z_1]^T, \quad l_2 = [x_2, y_2, z_2]^T, \quad l_3 = [x_3, y_3, z_3]^T \quad (6)$$

By the GRF approximation, z_1, z_2 , and z_3 are the random variables satisfying

$$\mathbb{E}[z_i] = \mu_i, \quad \mathbb{E}[(z_i - \mu_i)(z_j - \mu_j)] = \rho_{ij}, \quad i, j = 1, 2, 3 \quad (7)$$

where μ_i and ρ_{ij} are known. We can compute the slope and roughness by finding the landing surface, which is the plane spanned by the landing pads l_1, l_2 , and l_3 . The normal vector, n , of the landing surface is obtained by taking the cross product:

$$\begin{aligned} n &= (l_2 - l_1) \times (l_3 - l_1) \\ &= \begin{bmatrix} y_{12}(z_3 - z_1) - y_{13}(z_2 - z_1) \\ x_{13}(z_2 - z_1) - x_{12}(z_3 - z_1) \\ x_{12}y_{13} - x_{13}y_{12} \end{bmatrix} =: \begin{bmatrix} a \\ b \\ c \end{bmatrix} \end{aligned} \quad (8)$$

where $x_{ij} = x_j - x_i$ and $y_{ij} = y_j - y_i$. The slope s is defined as the angle between the normal vector n and the vertical axis, and the roughness $r(\gamma)$ is the distance between the terrain and the landing surface at the horizontal location of $\gamma \in U$, where U represents the set of horizontal coordinates within the lander footprint. The slope and roughness are then computed as

$$\begin{aligned} s &= \arccos\left(\frac{c}{\sqrt{a^2 + b^2 + c^2}}\right) \\ r(\gamma) &= \frac{|ax + by + cz + d|}{\sqrt{a^2 + b^2 + c^2}}, \quad \gamma = (x, y) \in U, \quad z = f(\gamma) \end{aligned} \quad (9)$$

where $z = f(\gamma)$ is the terrain elevation at γ , and d satisfies $ax_i + by_i + cz_i + d = 0$ for all $l_i = [x_i, y_i, z_i]^T$, $i = 1, 2$, and 3 . Given the slope and roughness thresholds \bar{s} and \bar{r} , the conditional probability of safety is expressed as follows.

$$\mathbb{P}\{\text{Safe}|\theta_o\} = \mathbb{P}\{s < \bar{s}, \text{ and } r(\gamma) < \bar{r} \text{ for all } \gamma \in U|\theta_o\} \quad (10)$$

Note that the computation of the conditional joint probability of Eq. (10) under Eqs. (7)(8)(9) is not straightforward because z_1, z_2, z_3 , and z are all correlated random variables. To ease the computation, we approximate the probability of safe landing by decomposing it into slope safety and roughness safety, as in Eq. (11).

$$\begin{aligned} \mathbb{P}\{\text{Safe}|\theta_o\} &= \mathbb{P}\{s < \bar{s}, \text{ and } r(\gamma) < \bar{r} \text{ for all } \gamma \in U|\theta_o\} \\ &\sim \mathbb{P}\{s < \bar{s}|\theta_o\} \mathbb{P}\{r(\gamma) < \bar{r} \text{ for all } \gamma \in U|\theta_o\} \end{aligned} \quad (11)$$

In the following subsections, we derive the analytical expressions of the conditional probability of slope safety, $\mathbb{P}\{s < \bar{s}|\theta_o\}$, and the conditional probability of roughness safety, $\mathbb{P}\{r(\gamma) < \bar{r} \text{ for all } \gamma \in U|\theta_o\}$.

Probability of Slope Safety

Here we derive the analytical form of the probability of slope safety, $\mathbb{P}\{s < \bar{s}|\theta_o\}$. Let us introduce the multivariate normal variable Z_s to represent the joint distribution of the elevations of the three landing pads contacting the terrain with the orientation angle θ_o .

$$Z_s := [z_1, z_2, z_3]^T \sim \mathcal{N}(\mu_s, \Sigma_s),$$

where $\mu_s \in \mathbb{R}^3$ and $\Sigma_s \in \mathbb{R}^{3 \times 3}$ are known by the GRF approximation. Then, we can rewrite the conditional probability of slope safety as follows.

$$\begin{aligned} \mathbb{P}\{s < \bar{s}|\theta_o\} &= \mathbb{P}\left\{a^2 + b^2 < c^2 \left(\frac{1}{\cos^2(\bar{s})} - 1\right)\right\} \\ &= \mathbb{P}\left\{Z_s^T A(\theta_o) Z_s < \tau_{\bar{s}}(\theta_o)\right\}, \end{aligned}$$

where

$$\begin{aligned} A(\theta_o) &= \begin{bmatrix} x_{23}^2 + y_{23}^2 & -x_{13}x_{23} - y_{13}y_{23} & x_{12}x_{23} + y_{12}y_{23} \\ -x_{13}x_{23} - y_{13}y_{23} & x_{13}^2 + y_{13}^2 & -x_{12}x_{13} - y_{12}y_{13} \\ x_{12}x_{23} + y_{12}y_{23} & -x_{12}x_{13} - y_{12}y_{13} & x_{12}^2 + y_{12}^2 \end{bmatrix}, \\ \tau_{\bar{s}}(\theta_o) &= c^2 \left(\frac{1}{\cos^2(\bar{s})} - 1\right) \end{aligned} \quad (12)$$

Note that both $A(\theta_o)$ and $\tau_{\bar{s}}(\theta_o)$ are constant and depends on the lander's orientation angle θ_o at touchdown. However, if we ignore the roughness safety and are only interested in the slope safety, we can make A invariant over θ_o by fixing the xy -coordinate with respect to the horizontal locations of the three landing pads, γ_1 , γ_2 , and γ_3 .

The probability of slope safety, derived as Eq. (12), is represented as the tail distribution of the quadratic form of the multivariate normal distribution. The quadratic form of the multivariate normal distribution is known as the generalized chi-squared distribution, which is a linear combination of independent non-central chi-square variables.⁷ Here we approximate the quadratic form of the multivariate normal distribution by the Gaussian distribution with the mean and the variance obtained as follows.⁷

$$\begin{aligned} m_s(\theta_o) &:= \mathbb{E}[Z_s^T A Z_s] = \text{tr}(A \Sigma_s) + \mu_s^T A \mu_s \\ \sigma_s^2(\theta_o) &:= \text{Var}[Z_s^T A Z_s] = 2\text{tr}(A \Sigma_s A \Sigma_s) + 4\mu_s^T A \Sigma_s A \mu_s \end{aligned} \quad (13)$$

Then, by using the cumulative distribution function for the standard normal distribution, $\Phi(\cdot)$, we can approximate the conditional probability of slope safety by

$$\mathbb{P}\{s < \bar{s}|\theta_o\} \sim \Phi\left(\frac{\tau_{\bar{s}}(\theta_o) - m_s(\theta_o)}{\sqrt{2}\sigma_s(\theta_o)}\right). \quad (14)$$

Probability of Roughness Safety

The precise computation of the conditional probability of roughness safety requires evaluating integrals for all the points beneath the lander. To ease the computation, we introduce the rasing factor $k_2 > 0$ to approximate the conditional probability by the worst-case roughness instance

within the landing footprint as in Eq. (15).

$$\begin{aligned}
\mathbb{P}\{r(\gamma) < \bar{r}, \text{ for all } \gamma \in U|\theta_o\} &= \int_{-\infty}^{\bar{r}} \cdots \int_{-\infty}^{\bar{r}} \mathbb{P}(r_1, \dots, r_{|U|}|\theta_o) dr_1 \cdots dr_{|U|} \\
&\sim \left[\min_{\gamma_p \in U} \int_{-\infty}^{\bar{r}} \mathbb{P}(r(\gamma_p)|\gamma_p, \theta_o) dr_p \right]^{k_2} \\
&= \left[\min_{\gamma_p \in U} \mathbb{P}\{r(\gamma_p) < \bar{r}|\gamma_p, \theta_o\} \right]^{k_2}, \quad \text{where } k_2 > 0
\end{aligned} \tag{15}$$

Since $0 < \Phi(\cdot) < 1$, larger k_2 corresponds to a conservative approximation. The proposed approximation with $k_2 = 1$ represents the case when the worst-case roughness being under the threshold guarantees the roughness safety for the other points within U . When $k_2 = |U|$, it represents the case where all the points in U are independent and have an equally large roughness.

Similarly to the slope case, let us introduce the multivariate normal variable $Z_r = [z_1, z_2, z_3, z_p]^T$ to represent the joint distribution of the four elevations; z_1, z_2 , and z_3 are the elevations of the three landing pads contacting the terrain surface with orientation angle θ_o , and $z_p = f(\gamma_p)$ is the elevation of an arbitral point within the lander footprint such that $\gamma_p = [x_p, y_p]^T \in U$. Then Z_r follows the multivariate normal distribution,

$$Z_r := [z_1, z_2, z_3, z_p]^T \sim \mathbf{N}(\mu_r, \Sigma_r),$$

where $\mu_r \in \mathbb{R}^4$ and $\Sigma_r \in \mathbb{R}^{4 \times 4}$ are known by the GRF approximation. With Z_r , we can rewrite the conditional probability of roughness safety for an arbitral point $\gamma_p \in U$, as follows.

$$\begin{aligned}
\mathbb{P}\{r(\gamma_p) < \bar{r}|\gamma_p, \theta_o\} &= \mathbb{P}\{(ax_p + by_p + cz_p + d)^2 < \bar{r}^2(a^2 + b^2 + c^2)\} \\
&= \mathbb{P}\{(ax_p + by_p + cz_p - ax_1 - by_1 - cz_1)^2 < \bar{r}^2(a^2 + b^2 + c^2)\} \\
&= \mathbb{P}\{(ax_{1p} + by_{1p} + c(z_p - z_1))^2 - \bar{r}^2(a^2 + b^2) < \bar{r}^2c^2\} \\
&= \mathbb{P}\{Z_r^T B(\gamma_p, \theta_o) Z_r < \tau_{\bar{r}}(\theta_o)\},
\end{aligned}$$

where

$$\begin{aligned}
\tau_{\bar{r}}(\theta_o) &= \bar{r}^2 c^2 \\
B(\gamma_p, \theta_o) &= [\beta_{ij}] \\
\beta_{11} &= (x_{1p}y_{23} - x_{23}y_{1p})^2 - \bar{r}^2(x_{23}^2 + y_{23}^2) + c^2 - 2c(x_{1p}y_{23} - x_{23}y_{1p}) \\
\beta_{22} &= (x_{1p}y_{13} - x_{13}y_{1p})^2 - \bar{r}^2(x_{13}^2 + y_{13}^2) \\
\beta_{33} &= (x_{1p}y_{12} - x_{12}y_{1p})^2 - \bar{r}^2(x_{12}^2 + y_{12}^2) \\
\beta_{44} &= c^2 \\
\beta_{12} = \beta_{21} &= -(x_{1p}y_{13} - x_{13}y_{1p})(x_{1p}y_{23} - x_{23}y_{1p} - c) + \bar{r}^2(x_{13}x_{23} + y_{13}y_{23}) \\
\beta_{13} = \beta_{31} &= (x_{1p}y_{12} - x_{12}y_{1p})(x_{1p}y_{23} - x_{23}y_{1p} - c) - \bar{r}^2(x_{12}x_{23} + y_{12}y_{23}) \\
\beta_{14} = \beta_{41} &= c(x_{1p}y_{23} - x_{23}y_{1p} - c) \\
\beta_{23} = \beta_{32} &= -(x_{1p}^2 - \bar{r}^2)y_{12}y_{13} - (y_{1p}^2 - \bar{r}^2)x_{12}x_{13} + x_{1p}y_{1p}(x_{12}y_{13} + x_{13}y_{12}) \\
\beta_{24} = \beta_{42} &= -c(x_{1p}y_{13} - x_{13}y_{1p}) \\
\beta_{34} = \beta_{43} &= c(x_{1p}y_{12} - x_{12}y_{1p}).
\end{aligned} \tag{16}$$

We used the relation $ax_1 + by_1 + cz_1 + d = 0$ to erase d . Note that both $B(\gamma_p, \theta_o)$ and $\tau_{\bar{r}}(\theta_o)$ are constant.

Analogously to the slope safety, we approximate the derived conditional probability by its mean and variance. Finally, we obtain the following approximation about the conditional probability of roughness safety.

$$\begin{aligned} \mathbb{P}\{r(\gamma_p) < \bar{r}|\gamma_p, \theta_o\} &\sim \Phi\left(\frac{\tau_{\bar{r}}(\theta_o) - m_r(\theta_o)}{\sqrt{2}\sigma_r(\theta_o)}\right), \quad \text{where} \\ m_r(\theta_o) &:= \mathbb{E}[Z_r^T B Z_r] = \text{tr}(B\Sigma_r) + \mu_r^T B \mu_r \\ \sigma_r^2(\theta_o) &:= \text{Var}[Z_r^T B Z_r] = 2\text{tr}(B\Sigma_r B\Sigma_r) + 4\mu_r^T B\Sigma_r B \mu_r \end{aligned} \quad (17)$$

Stochastic Hazard Detection Algorithm

Algorithm 1 shows the resulting stochastic hazard detection algorithm that takes the GRF representation of the approximated terrain, and returns the probability of slope safety and the probability of roughness safety for each point on the terrain. For efficient implementation, the matrices $A(\theta_o)$ and $B(\gamma_p, \theta_o)$ in Eqs. (12)(16) should be precomputed. Note that A and B can be reused for different targets by taking the target-centered coordinates, so the number of A and B matrices to be precomputed are $|\Theta|$ and $|U||\Theta|$, respectively.

If we have a fourth landing pad, we check if the fourth landing pad is above the landing surface; given the fourth landing pad location, $l_4 = [x_4, y_4, z_4]$, we skip θ_o if $z_4 < (-ax_4 - by_4 - d)/c$. Although a, b, d , and z_4 are correlated random variables, we can use the expected value for the approximated feasibility check. To be conservative, we can replace z_4 as $z_4 \leftarrow \mathbb{E}[z_4] - 3\sqrt{\text{Var}[z_4]}$.

Algorithm 1 Stochastic Hazard Detection

Input: GRF representation of terrain

Output: Probabilistic safety map

Precompute A matrices of Eq. (12) for all $\theta_o \in \Theta$

Precompute B matrices of Eq. (16) for all $\gamma_p \in U$ and $\theta_o \in \Theta$

for Targets in DEM **do**

for Orientation angles $\theta_o \in \Theta$ **do**

 Evaluate $\mathbb{P}\{s < \bar{s}|\theta_o\}$ by Eq. (14)

 Update $\min_{\theta_o \in \Theta} [\mathbb{P}\{s < \bar{s}|\theta_o\}]$ for the target

for Terrain under lander footprint $\gamma_p \in U$ **do**

 Evaluate $\mathbb{P}\{r(\gamma_p) < \bar{r}|\gamma_p, \theta_o\}$ by Eq. (17)

 Update $\min_{\gamma_p \in U, \theta_o \in \Theta} [\mathbb{P}\{r(\gamma_p) < \bar{r}|\gamma_p, \theta_o\}]$ for the target

end for

end for

Store $\mathbb{P}^*\{s < \bar{s}\} := \min_{\theta_o \in \Theta} [\mathbb{P}\{s < \bar{s}|\theta_o\}]$ for the target

Store $\mathbb{P}^*\{r < \bar{r}\} := \min_{\gamma_p \in U, \theta_o \in \Theta} [\mathbb{P}\{r(\gamma_p) < \bar{r}|\gamma_p, \theta_o\}]$ for the target

end for

Adjust the probabilities by the rasing factors k_1 and k_2 with Eqs. (5)(15)

EXPERIMENTS AND RESULTS

Experiment Configurations

We evaluated the proposed algorithm on the HiRISE digital terrain model (DTM) of the candidate ExoMars landing site in Hypanis Valles.⁸ We cropped the DTM into 100 DEMs with the size of 32x32 at the maximum resolution of 1 meter per pixel (mpp). We evaluated these DEMs to obtain the true slope and roughness value per pixel. Here we assumed a triangular geometry of the lander with the diameter of 10 meters. To simulate the sparse LiDAR measurements, we downsampled the DEMs with the GSD of 1.5, 2, 3, 4 meters with the Gaussian elevation noise $\epsilon \sim N(0, \sigma^2)$ where $3\sigma = 5\text{cm}$. The simulated sparse LiDAR measurements are upsampled by fitting the GRF regressor of Eq. (3).

Given the sparse measurements and the associated GRFs, We evaluated the slope and roughness safety by three different models: the baseline model, the GRF-sampling model, and the stochastic hazard detection (SHD) model. The baseline model reconstructs the high-resolution DEMs via bilinear interpolation, and deterministically measure the slope and roughness. The GRF-sampling model numerically samples 100 high-resolution DEMs from the GRF, and obtain the probability of safety as the sample mean of the deterministic evaluations. The SHD model takes the GRF and analytically approximate the probability of safety, as described in the previous section.

Table 1. Optimal raising factors of Eqs. (5)(16).

Raising Factor	GSD			
	1.5m	2.0m	3.0m	4.0m
k_1	3.00	3.64	4.91	5.91
k_2	0.42	0.74	1.04	1.09
$k_1 k_2$	1.27	2.71	5.11	6.45

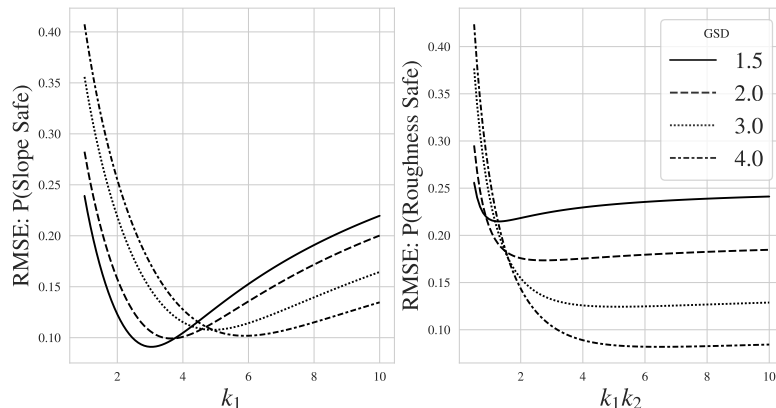


Figure 4. Approximation errors of the proposed analytical forms: Eqs. (5)(14)(17). GSD is in meters.

Accuracy of Derived Analytical Probabilities

To capture the approximation errors of the proposed analytical forms of Eqs. (5)(14)(17), Figure 4 shows the root-mean-squared error (RMSE) of the probabilities of slope safety and roughness safety,

between the analytical forms and the sample means over different raising factors k_1 and k_1k_2 . Note that the probability of roughness safety has the raising factor of k_1k_2 due to Eqs. (5)(17). The proposed analytical forms achieve the minimum RMSE of about 0.10 for the probability of slope safety, and from about 0.05 to 0.32 for the probability of roughness safety. As GSD increases, the optimal raising factors k_1 and k_2 increase for both slope and roughness probabilities, and RMSE of roughness-safe probability decreases. As shown later, this is related to the results that the probability of safety gets smaller for larger GSD due to the increased uncertainty, and the mean probability of roughness-safety approaches close to zero. Table 1 reports the optimal raising factors minimizing RMSE. We used the optimal raising factors for the following results.

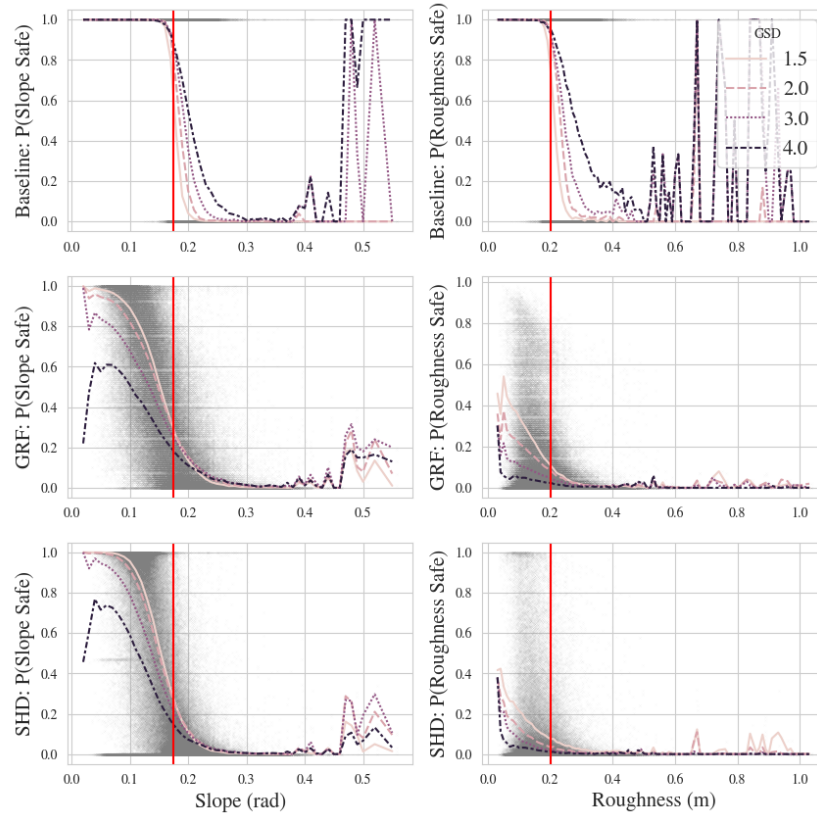


Figure 5. Distribution of the estimated safety probability by the baseline, the GRF-sampling model, and the SHD model, from top to bottom. Vertical red lines denote the safety thresholds. The line plots show the mean estimated safety probabilities given. The baseline is a deterministic model, and the estimated safeties are located at either 1 or 0.

Prediction Performance of Proposed Approach

Figure 5 shows the distribution of the estimated safety probability by the baseline, the GRF-sampling model, and the SHD model, from top to bottom. Line plots show the mean estimated

probability for different GSD cases. The baseline model has estimated safety probabilities of either 1 or 0, as it is a deterministic algorithm. The baseline algorithm fails to detect hazards from noisy, sparse inputs, resulting in the larger mean probabilities of safety on the right of the vertical red lines, which denotes the safety thresholds. Higher GSD inputs result in more missed hazards, represented by the increased safety probability in the region over the thresholds.

On the other hand, the GRF-sampling model and the SHD model successfully assign lower safety probabilities than the baseline to hazardous targets. We can also observe the distributions of the GRF-sampling and SHD models overlaps, showing the precision of the derived analytical approximations. Note that the raising factors k_1 and k_2 are constant over the same GSD inputs, and their optimization cannot arbitrarily change the distribution; it only compresses the SHD distributions vertically.

The GRF-sampling model and the SHD model both assign larger safety probabilities to less hazardous targets, and their safety probability decreases for larger input GSDs due to the increased uncertainty. The mean estimated probabilities of roughness safety are kept relatively low even for the safe targets, and approach close to zero with larger GSDs. This means roughness safety is more sensitive to the topographic uncertainty than slope safety.

Qualitative Safety Mapping Results

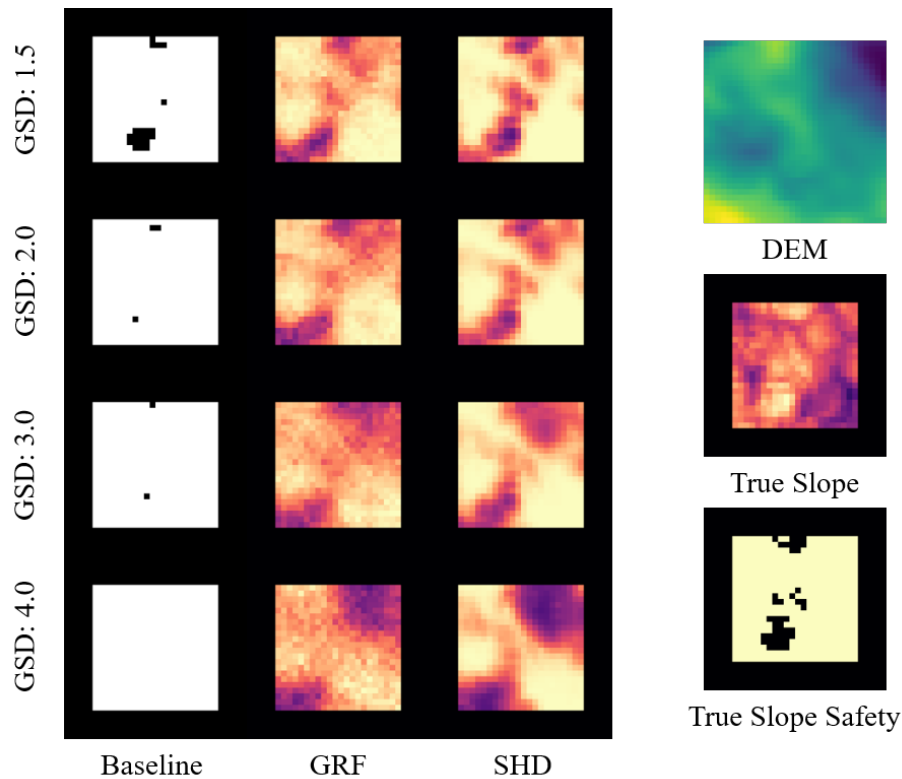


Figure 6. Estimated slope safety maps. The brighter pixels correspond to safe targets for the true safety map, and the estimated safety probability for the baseline, GRF-sampling, and SHD model predictions. The brighter pixels of the DEM and the true slope map correspond to their higher values.

Figures 6 and 7 show the estimated safety probability maps for slope and roughness, respectively. The baseline predictions miss landing hazards, denoted by black pixels, especially for higher GSD inputs. Compared to the baseline, the GRF-sampling and SHD models successfully capture the landing hazards even for higher GSD inputs, which illustrates that the GRF-sampling and SHD models allow successful hazard detection operations from noisy, sparse terrain observations.

Comparing the GRF and SHD models, the SHD model is less noisy and has more sharp boundaries of safety, especially for the larger GSD inputs. This is because the SHD model is based on the analytical expressions of estimated probability, instead of the safety samples as in the GRF-sampling model; for the larger GSD inputs, the increased uncertainty decreases the sample efficiency with respect to the precise probability estimation. However, the analytical expressions of SHD can minimize this effect and enables less noisy probability estimations.

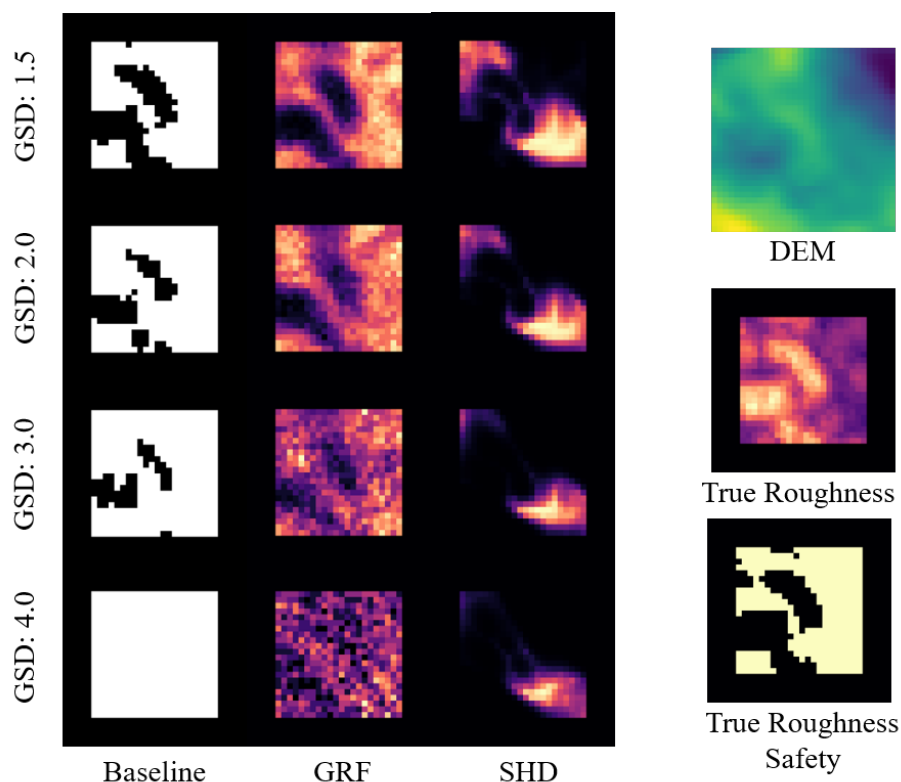


Figure 7. Estimated roughness safety maps. The brighter pixels correspond to safe targets for the true safety map, and the estimated safety probability for the baseline, GRF-sampling, and SHD model predictions. The brighter pixels of the DEM and the true roughness map correspond to their higher values.

CONCLUSION

We proposed a new stochastic hazard detection (HD) algorithm capable of more general topographic uncertainty by leveraging the Gaussian random field (GRF) regression. Given the noisy, sparse topographic observations, we demonstrated the GRF-based HD algorithm can detect landing hazards that are missed by the bilinear-interpolation-based algorithm. Further, we derived the analytical approximations of the safety probability and demonstrated the accuracy of the derived

expressions. The numerical experiments with the existing Mars terrain model showed the analytical evaluation of the safety probability is more robust to the increased topographic uncertainty than the sampling based algorithm. We demonstrated that the proposed approach enables the safety assessment with imperfect and sparse sensor measurements, which allows hazard detection operations under more diverse conditions.

ACKNOWLEDGMENTS

This work is supported by the National Aeronautics and Space Administration under Grant No.80NSSC20K0064 through the NASA Early Career Faculty Program.

REFERENCES

- [1] T. Ivanov, A. Huertas, and J. M. Carson, "Probabilistic hazard detection for autonomous safe landing," *AIAA Guidance, Navigation, and Control (GNC) Conference*, 2013, p. 5019.
- [2] K. Tomita, A. K. Skinner, and K. Ho, "Bayesian Deep Learning for Segmentation for Autonomous Safe Planetary Landing," *J. of Spacecraft and Rockets*, 2022, <https://doi.org/10.2514/1.A35104>.
- [3] C. I. Restrepo, P.-T. Chen, R. R. Sostaric, and J. M. Carson, "Next-generation nasa hazard detection system development," *AIAA Scitech 2020 Forum*, 2020, p. 0368.
- [4] M. Seeger, "Gaussian processes for machine learning," *International journal of neural systems*, Vol. 14, No. 02, 2004, pp. 69–106.
- [5] B. D. Malamud and D. L. Turcotte, "Wavelet analyses of Mars polar topography," *Journal of Geophysical Research: Planets*, Vol. 106, No. E8, 2001, pp. 17497–17504.
- [6] D. L. Turcotte, "A fractal interpretation of topography and geoid spectra on the Earth, Moon, Venus, and Mars," *Journal of Geophysical Research: Solid Earth*, Vol. 92, No. B4, 1987, pp. E597–E601.
- [7] A. C. Rencher and G. B. Schaalje, *Linear models in statistics*. John Wiley & Sons, 2008.
- [8] A. S. McEwen, E. M. Eliason, J. W. Bergstrom, N. T. Bridges, C. J. Hansen, W. A. Delamere, J. A. Grant, V. C. Gulick, K. E. Herkenhoff, L. Keszthelyi, R. L. Kirk, M. T. Mellon, S. W. Squyres, N. Thomas, and C. M. Weitz, "Mars reconnaissance orbiter's high resolution imaging science experiment (HiRISE)," *Journal of Geophysical Research E: Planets*, Vol. 112, 5 2007, 10.1029/2005JE002605.